Appl Phys B (2011) 103:537–546
DOI 10.1007/s00340-011-4375-9

Applied Physics B
Lasers and Optics

Two-dimensional array of room-temperature nanophotonic logic gates using InAs quantum dots in mesa structures

T. Kawazoe · M. Ohtsu · S. Aso · Y. Sawado · Y. Hosoda · K. Yoshizawa · K. Akahane · N. Yamamoto · M. Naruse

Received: 22 December 2010 / Published online: 10 February 2011

Abstract By growing two layers of InAs quantum dots on a substrate and processing the substrate to form mesa structures, we successfully fabricated for the first time nanophotonic devices that operate at room temperature. We fabricated two types of two-dimensional mesa arrays. The mesa dimensions of the individual arrays were 300 nm × 300 nm × 85 nm and 200 nm × 200 nm × 85 nm, and the areal density was 1×10^8 cm^{-2}. By adjusting the characteristics of energy transfer via dressed photons between two InAs quantum dots in the upper and lower layers of the mesa structures, we implemented devices that operate as AND gates and NOT gates. We fabricated 133 devices (with mesa dimensions of 300 nm on each side), of which 53 devices operated as AND gates and 50 devices operated as NOT gates.

T. Kawazoe (✉) · M. Ohtsu · M. Naruse
Department of Electrical Engineering and Information Systems, Graduate School of Engineering, The University of Tokyo, 2-11-16 Yayoi, Bunkyo-ku, Tokyo 113-8656, Japan
e-mail: kawazoe@ee.t.u-tokyo.ac.jp
Fax: +81-3-5841-1140

T. Kawazoe · M. Ohtsu
Nanophotonic Research Center, Graduate School of Engineering, The University of Tokyo, 2-11-16 Yayoi, Bunkyo-ku, Tokyo 113-8656, Japan

S. Aso · Y. Sawado · Y. Hosoda · K. Yoshizawa
Pioneer Corporation, 465 Osato-cho, Kofu-shi, Yamanashi 400-0053, Japan

K. Akahane · N. Yamamoto · M. Naruse
National Institute of Information and Communications Technology, Koganei, Tokyo 184-8795, Japan

K. Akahane · N. Yamamoto · M. Naruse
The University of Tokyo, 2-11-16 Yayoi, Bunkyo-ku, Tokyo 113-8656, Japan

1 Introduction

New nanoscale photonic devices [1–6] and nanoscale fabrication methods [7–10] based on near-field optical interactions through exchange of dressed photons between nanoscale matter have been realized. Dressed photons are virtual quasi-particles representing quantum states in which light is combined with an elementary excitation of matter [1]. A nanoscale optical device that uses dressed photons as signal carriers, i.e., a nanophotonic device, has the following features: (i) The device dimensions are considerably smaller than the wavelength of light. (ii) Since it is possible to utilize electric dipole-forbidden transitions, the loss due to recombination of the elementary excitation is reduced [11]. (iii) Energy consumption is drastically reduced compared with conventional devices [6].

Various types of nanophotonic devices have been proposed, and their operations have been verified, such as AND gates [2, 3], NOT gates [4], XOR gates [12], and optical nanofountains [13] implemented by using quantum dots (QDs) of CuCl, ZnO, or InGaAs. However, these devices were only able to operate at low temperatures below the temperature of liquid nitrogen.

In this research, in order to overcome this shortcoming, we processed two layers of InAs QDs having a low areal density into mesa structures to fabricate AND gates and NOT gates. As a result, of 133 devices (with mesa dimensions of 300 nm on each side) we fabricated, 53 AND gates and 50 NOT gates successfully operated at room temperature.

2 Structure and principles of the devices

Figure 1(a) shows the cross-sectional structure of a nanophotonic device formed of two InAs QDs (QD1, QD2) aligned

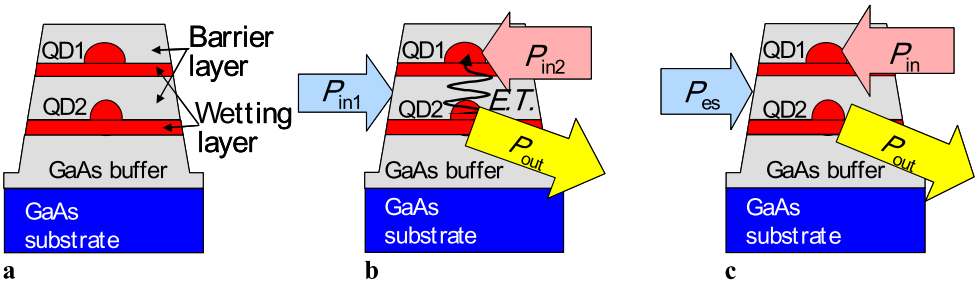

Fig. 1 The structure of a nanophotonic device. (**a**) A nanophotonic device formed of two quantum dots QD1 and QD2 having different sizes. (**b**) AND gate. (**c**) NOT gate

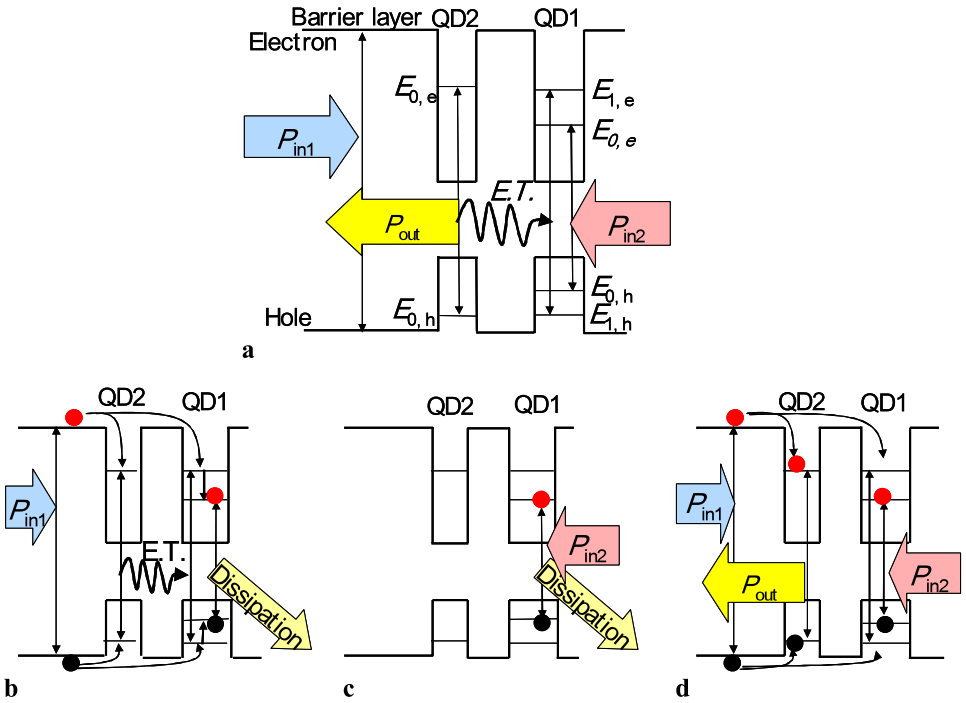

Fig. 2 Energy diagram of QD1 and QD2 that operate as an AND gate by resonance between E(QD1:$E_{1,e}$–$E_{1,h}$) and E(QD2:$E_{0,e}$–$E_{0,h}$). E.T. denotes energy transfer via dressed photons. *Red circles* represent electrons, and *black circles* represent holes. (**a**) Low state ($P_{out} = 0$; $P_{in1} \neq 0$, $P_{in2} = 0$), (**b**) low state ($P_{out} = 0$; $P_{in1} = 0$, $P_{in2} \neq 0$), and (**c**) high state ($P_{out} \neq 0$; $P_{in1} \neq 0$, $P_{in2} \neq 0$)

vertically and having different sizes. These QDs are located in barrier layers in a mesa structure. The barrier layers are thick enough that the wave functions representing the electronic states of the two QDs do not overlap but are thin enough that dressed photons can be exchanged [1]. Figures 2(a) and 3(a) show the quantized energy levels $E_{n,e}$ and $E_{n,h}$ ($n = 0, 1$) of electrons and holes in the two QDs. An electronic transition between $E_{n,e}$ and $E_{n,h}$ will be referred to as an $E_{n,e}$–$E_{n,h}$ transition. The energies that are absorbed or released with the $E_{n,e}$–$E_{n,h}$ transition of QD1 and QD2 (transition energies) will be denoted as E(QD1:$E_{n,e}$–$E_{n,h}$) and E(QD2:$E_{n,e}$–$E_{n,h}$), respectively. Electric dipole-allowed transitions in QD1 and QD2 are the $E_{0,e}$–$E_{0,h}$ transition and the $E_{1,e}$–$E_{1,h}$ transition [14–16]. An AND gate operation is achieved by controlling the energy levels ($E_{n,e}$, $E_{n,h}$) such that the transition energies E(QD1:$E_{1,e}$–$E_{1,h}$) and E(QD2:$E_{0,e}$–$E_{0,h}$) of the two QDs are resonant with each other. On the other hand, in the case where the transition energies E(QD1:$E_{1,e}$–$E_{1,h}$) and E(QD2:$E_{0,e}$–$E_{0,h}$) are slightly off-resonant, if the difference between these energies is not so large, the energy linewidths increase by the many-body effect [4], causing these energies to become resonant with each other. Thus, a NOT gate operation is achieved in this case. In short, it is possible to implement two types of nanophotonic devices that operate in different ways by controlling the energy levels ($E_{n,e}$, $E_{n,h}$).

1. Resonant case: The device operates as an AND gate [2, 4] (Figs. 1(b) and 2). Two input light signals (whose powers are denoted by P_{in1} and P_{in2}) generate electron–hole pairs (e–h pairs) in the barrier layer and QD1 serving as input terminals, respectively. The e–h pairs generated in the barrier layer undergo intraband relaxation and then reach the $E_{0,h}$–$E_{0,e}$ level of QD1 or QD2. QD2 serves as an output terminal. The wavy arrows E.T. in the figures represent energy transfer from QD2 to QD1 via dressed photons. At QD2 serving as an output terminal, electrons and holes recombine through the $E_{0,e}$–$E_{0,h}$ transition in QD2 to generate an output light signal (whose power is denoted by P_{out}).

(i) $P_{in1} \neq 0$, $P_{in2} = 0$ (Fig. 2(b)): The electrons and holes generated in the barrier layer undergo intraband relaxation

while moving to QD1 or QD2. Then, the electrons and holes relax to the levels $E_{0,e}$ and $E_{0,h}$ of QD2, respectively. The $E_{0,e}$–$E_{0,h}$ transition energy $E(\mathrm{QD2}{:}E_{0,e}{-}E_{0,h})$ of the e–h pairs is transferred to QD1 by resonance via dressed photons (E.T. in Fig. 2(b)). Furthermore, the electrons and holes of the e–h pairs undergo inter-sublevel relaxation to the levels $E_{0,e}$ and $E_{0,h}$ of QD1, respectively, and the e–h pairs vanish by recombination of the electrons and holes, whereby the energy input to the device as P_{in1} is dissipated from QD1. Thus, no output signal is generated ($P_{out} = 0$: low state).

(ii) $P_{in1} = 0$, $P_{in2} \neq 0$ (Fig. 2(c)): The e–h pairs generated in QD1 vanish by the $E_{0,e}$–$E_{0,h}$ transition, so that no output signal is generated ($P_{out} = 0$: low state).

(iii) $P_{in1} \neq 0$, $P_{in2} \neq 0$ (Fig. 2(d)): The e–h pairs generated in the barrier layer move to QD1 or QD2 and undergo inter-sublevel relaxation. Of the e–h pairs, the transition energy $E(\mathrm{QD2}{:}E_{0,e}{-}E_{0,h})$ of the e–h pairs in QD2 is prohibited from transferring to QD1. This is because the energy levels of electrons and holes in QD1 are already occupied by electrons and holes generated by P_{in1}. The transition energy $E(\mathrm{QD2}{:}E_{0,e}{-}E_{0,h})$ of QD2, which is prohibited from transferring, is released by recombination of electrons and holes through the $E_{0,e}$–$E_{0,h}$ transition. As a result, an output signal is generated ($P_{out} \neq 0$: high state).

2. Slightly off-resonant case: The device operates as a NOT gate [4] (Figs. 1(c) and 3). Light, as the energy source, enters the NOT gate. This light energy is supplied to the barrier layer (same as P_{in1} in case 1, denoted by P_{es} here). QD1 serves as an input terminal. An input signal (same as P_{in2} in case 1, denoted by P_{in} here) generates e–h pairs through the $E_{0,e}$–$E_{0,h}$ transition in QD1. QD2 serves as an output terminal, where electrons and holes recombine through the $E_{0,e}$–$E_{0,h}$ transition in QD2 to generate an output light signal (P_{out}).

(i) $P_{in} = 0$ (Fig. 3(b)): The electrons and holes generated in the barrier layer by the light (P_{es}) serving as an energy source move to QD1 and QD2 while undergoing intraband relaxation. The electrons and holes moved to QD1 undergo inter-sublevel relaxation to the levels $E_{0,e}$ and $E_{0,h}$ in QD1, respectively, and then the e–h pairs vanish through the $E_{0,e}$–$E_{0,h}$ transition. Since $E(\mathrm{QD2}{:}E_{0,e}{-}E_{0,h})$ is not resonant with $E(\mathrm{QD1}{:}E_{1,e}{-}E_{1,h})$, the e–h pairs moved to QD2 are prohibited from moving to QD1 and vanish by recombination of the electrons and holes. Thus, an output signal is generated ($P_{out} \neq 0$: high state).

(ii) $P_{in} \neq 0$ (Fig. 3(c)): Since the linewidths of energy levels of QD1 increase by the many-body effect [4], $E(\mathrm{QD1}{:}E_{1,e}{-}E_{1,h})$ and $E(\mathrm{QD2}{:}E_{0,e}{-}E_{0,h})$ come to be resonant with each other. At this time, the e–h pairs generated in the barrier layer by the light serving as an energy source move to QD2 while undergoing intraband relaxation. The transition energy $E(\mathrm{QD2}{:}E_{0,e}{-}E_{0,h})$ of the e–h pairs can transfer to QD1 by resonance (E.T. in Fig. 3(c)). As a result, the e–h pairs in QD2 vanish, so that no output signal is generated ($P_{out} = 0$: low state).

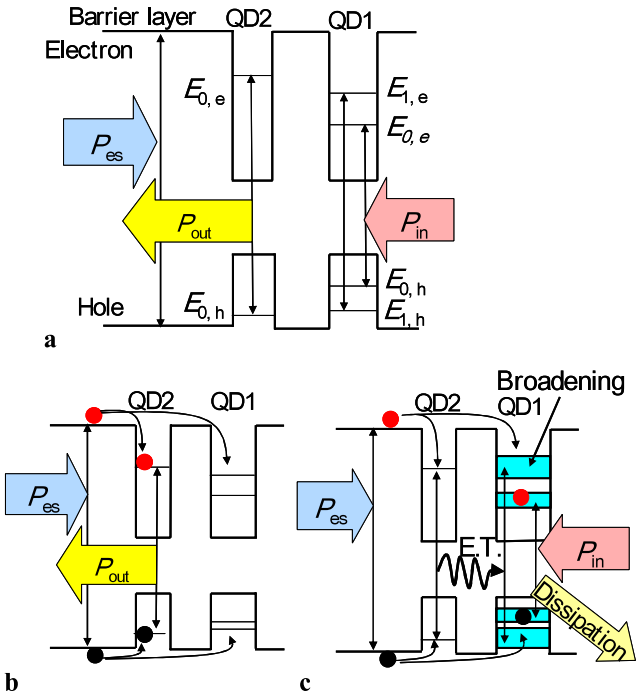

Fig. 3 Energy diagram of QD1 and QD2 in the case where $E(\mathrm{QD1}{:}E_{1,e}{-}E_{1,h})$ and $E(\mathrm{QD2}{:}E_{0,e}{-}E_{0,h})$ are slightly off-resonant, and QD1 and QD2 operate as a NOT gate. (**a**) High state ($P_{out} \neq 0$; $P_{in} = 0$) and (**b**) low state ($P_{out} = 0$; $P_{in} \neq 0$)

3 Fabrication and evaluation

We used a GaAs wafer as a substrate and grew InAs QDs on the substrate by molecular beam epitaxy (MBE). Figure 4(a) shows the cross-sectional structures of a buffer layer, barrier layers, wetting layers, and QDs grown on the GaAs substrate. The requirements for realizing room-temperature operation and a method we discovered for satisfying the requirements are as follows: (i) Ability to precisely control the distances between QDs (the distance between two QDs constituting a device should be less than or equal to the diameter of a QD, and distances with respect to the other QDs should be greater than the diameter of a QD): By utilizing the phenomenon in which QDs align vertically as a result of growth in the Stranski–Krastanov mode [17], only QDs in the upper layer and the lower layer were placed in proximity to each other. We adjusted the distance between the QDs by controlling the thickness of the barrier layers. Furthermore, we made the areal density of QDs in each layer low by controlling the growth rate. (ii) Satisfying the resonant and slightly off-resonant device operating conditions, described

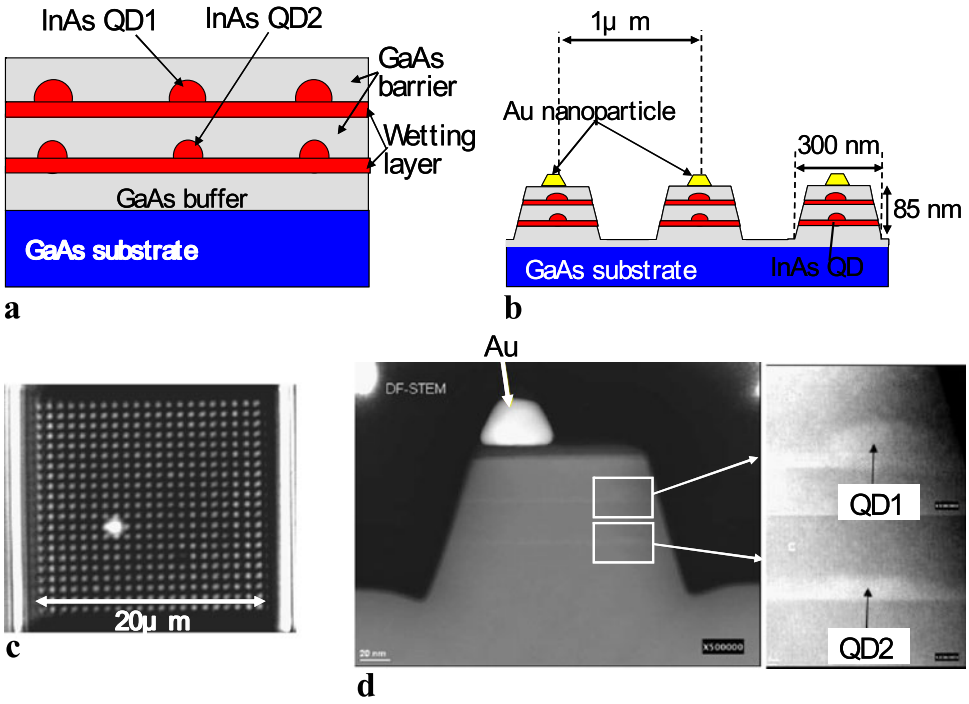

Fig. 4 Mesa structure fabricated by using two layers of InAs QDs. (**a**) The structure of two layers of InAs QDs used for mesa processing. (**b**) A cross-section of the mesa structure. (**c**) Image of the entire two-dimensional array of mesa structures, taken with an optical microscope. (**d**) Cross-sectional image of a mesa, taken with a scanning transmission electron microscope (S-TEM)

in 1 and 2 above, by controlling the quantized energy levels of QD1 and QD2: We controlled the growth rate and deposition thickness of QDs. (iii) Sufficiently high quantum efficiency of photoluminescence at room temperature: We controlled the heating rate under As-source irradiation and the growth temperature of the barrier layers.

The fabrication process satisfying the above requirements (i) to (iii) is as follows. First, we grew a GaAs buffer layer having a thickness of 150 nm on the substrate. Then, we grew 1.8 monolayers of QD2 on the buffer layer (growth temperature, 510°C). Then, we grew a GaAs layer (barrier layer) having a thickness of 24 nm (growth temperature, 475°C) and then grew 1.8 monolayers of QD1 (growth temperature, 510°C). Finally, we grew a GaAs layer (barrier layer) having a thickness of 24 nm (growth temperature, 440°C).

Figure 4(b) shows the cross-sectional structure of the two-dimensional mesa array we fabricated. After fabricating a Ti mask on the quantum dots fabricated as described above by the lift-off method using electron-beam lithography, we formed two-dimensional arrays of two types of mesa devices by Ar-ion milling. The dimensions of the bottom of each mesa structure were 300 nm × 300 nm (Fig. 4(b)) and 200 nm × 200 nm, and the height was 85 nm. The average number of pairs of QD1 and QD2 in each mesa structure, estimated on the basis of the areal density of QDs mentioned earlier, was 4.0 for the 300 nm-size mesa structures and 1.5 for the 200 nm-size mesa structures. We arrayed 20 × 20 mesa devices two-dimensionally at intervals of 1 μm (areal density of 1×10^8 cm^{-2}). Figure 4(c) shows an image of the two-dimensional array, taken with an optical microscope.

Figure 4(d) shows a cross-sectional image of the device, taken with a scanning transmission electron microscope (S-TEM). It will be understood that QD1 is located directly above QD2 and that the distance between QD1 and QD2 is controlled by the thickness of the barrier layer. As will be understood from the image, QD1 and QD2 are aligned vertically, separated by a barrier layer having a thickness of 24 nm. The average dimensions of QD1 were 42 nm in diameter and 11 nm in height. The average dimensions of QD2 were 38 nm in diameter and 10 nm in height. The areal density of QDs was 1.0×10^{10} cm^{-2}. Since the average in-plane interval was 100 nm, requirement (i) was satisfied. Furthermore, as is shown in the image, an Au nanoparticle having a diameter of 50 nm and a height of 30 nm was provided on top of the mesa structure. The Au nanoparticle on the mesa structure was also fabricated by Ar-ion milling using a Ti mask. The Au nanoparticle has the role of improving the efficiency of outputting propagating light as an output signal of the device. That is, since GaAs constituting the barrier layer has a large refractive index, light signals emitted by the device are scattered backward in the direction of the substrate [18]. At this time, the Au nanoparticle serves to discharge a greater portion of the scattered light to the outside of the device.

The white squares in Fig. 5 represent measured values of the spectrum of light emitted by the fabricated QD1 and QD2 at room temperature (300 K). The solid curve is composed of multiple Gaussian curves, representing the result of fitting the measured values. As an excitation light source, we used second harmonic generation (SHG) light of

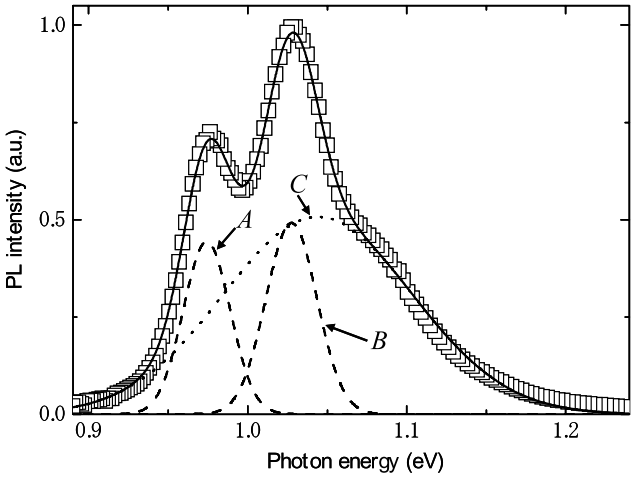

Fig. 5 Spectra of light emitted by the two layers of InAs QDs used for device fabrication. The *curve A* represents the spectrum of light emitted by recombination of electrons and holes through the transition $E_{0,e}$–$E_{0,h}$ in QD1. The *curve B* represents the spectrum in which the spectra of light emitted by recombination of electrons and holes through the transition $E_{1,e}$–$E_{1,h}$ in QD1 and the transition $E_{0,e}$–$E_{0,h}$ in QD2 overlap each other. The *curve C* represents the spectrum of light emitted from wetting layers

an Nd:YAG laser that emits light having a wavelength of 532 nm and an excitation intensity of 20 W/cm^2. We fitted the spectral component of light emitted by recombination of electrons and holes through the $E_{0,e}$–$E_{0,h}$ transition of QD1 with a Gaussian curve *A*. The peak energy of the spectrum (E(QD1:$E_{0,e}$–$E_{0,h}$)) was 0.974 eV, and the inhomogeneous linewidth of the spectrum was 28 meV. Furthermore, the spectra of light emitted by recombination of electrons and holes through the $E_{1,e}$–$E_{1,h}$ transition of QD1 and the $E_{0,e}$–$E_{0,h}$ transition of QD2 overlapped each other, and we fitted the spectra with a Gaussian curve *B*. The peak energy of the spectra (E(QD1:$E_{1,e}$–$E_{1,h}$) and E(QD2:$E_{0,e}$–$E_{0,h}$)) was 1.027 eV, and the inhomogeneous linewidth of the spectra was 31 meV. Furthermore, the curve *C* represents a broad spectrum of light emitted from the wetting layers. The inhomogeneous linewidth of the spectrum was 119 meV. The sources of these spectra were estimated from the spectra of light emitted from samples in which only QD2 were fabricated and samples in which only QD1 were fabricated and the results of measurement of dependency of these samples on the excitation intensity. The average value of the full width at half maximum (FWHM) of the spectrum of light emitted from a single QD at room temperature, measured by the microscopic photoluminescence method (μ-PL method), was 16 meV. The photoluminescence linewidth obtained from this spectrum substantially coincided with results obtained through other measurements of emitted light [19] and hole burning spectroscopy [20] and can be regarded as the homogeneous linewidth.

Based on the homogeneous linewidth and inhomogeneous linewidth, it is possible to obtain the probability of existence of QD pairs in which E(QD1:$E_{1,e}$–$E_{1,h}$) and E(QD2:$E_{0,e}$–$E_{0,h}$) are resonant with each other. We assumed that E(QD1:$E_{1,e}$–$E_{1,h}$) and E(QD2:$E_{0,e}$–$E_{0,h}$) were resonant with each other when the overlapping area of the homogeneous spectral broadenings of these transition energies was greater than half the area of the homogeneous spectral broadening of each one individually. Since the homogeneously broadened spectral shapes of light emitted from E(QD1:$E_{1,e}$–$E_{1,h}$) and E(QD2:$E_{0,e}$–$E_{0,h}$) of a single QD are represented by Lorentzian curves, E(QD1:$E_{1,e}$–$E_{1,h}$) and E(QD2:$E_{0,e}$–$E_{0,h}$) are considered as resonant if the distance between the positions of the spectral peaks of these energies is less than the FWHM (16 meV). On the other hand, since the Gaussian linewidth of the inhomogeneously broadened photoluminescence generated with E(QD1:$E_{1,e}$–$E_{1,h}$) and E(QD2:$E_{0,e}$–$E_{0,h}$) as described above is 31 meV, the probability of existence of a QD pair in which E(QD1:$E_{1,e}$–$E_{1,h}$) and E(QD2:$E_{0,e}$–$E_{0,h}$) are resonant with each other is expressed by

$$P(\delta x_c, x_h) = \int_0^\infty \int_{x_c}^{x_c+\delta x_c} \exp\left\{-\frac{(x+x_c)^2}{x_h^2}\right\} dx\, dx_c \Big/ \int_0^\infty \int_{x_c}^{\infty} \exp\left\{-\frac{(x+x_c)^2}{x_h^2}\right\} dx\, dx_c. \quad (1)$$

In this equation, the integration variables x and x_c represent photon energies, δx_c represents the homogeneous linewidth, and x_h represents the inhomogeneous linewidth. Assigning the above values, i.e., $\delta x_c = 16$ meV and $x_h = 31$ meV, the value of (1) is $P_1 \equiv P(16\text{ meV}, 31\text{ meV}) = 39\%$. Furthermore, we observed the dependency of the spectrum of light emitted by a single QD on the excitation intensity and confirmed that the homogeneous linewidth increased by 2.2 times or more by the many-body effect. Thus, if e–h pairs exist in a QD, the homogeneous linewidth would increase to at least 16 meV × 2.2 = 35 meV. At this time, by assigning $\delta x_c = 16$ meV and $x_h = 31$ meV in (1), it is found that the probability of existence of a resonant QD pair increases to $P_2 \equiv P(35\text{ meV}, 31\text{ meV}) = 74\%$. This indicates that QD pairs corresponding to the 35% difference from P_1 experienced a change from the off-resonant to resonant condition by excitation of E(QD1:$E_{1,e}$–$E_{1,h}$) and E(QD2:$E_{0,e}$–$E_{0,h}$). That is, this indicates that 35% of the QD pairs are slightly off-resonant and thus can operate as NOT gates. From the above discussion, it will be understood that requirement (ii) is satisfied by using the fabricated InAs QDs and that at least 74% of the QD pairs operate as AND gates or NOT gates.

When growing the barrier layer after growing quantum dots by MBE, we raised the temperature of the growth substrate to the growth temperature of the barrier layer under As irradiation. We suppressed diffusion of In by controlling the heating rate and the growth temperature of the barrier layer.

As a result, formation of nonradiative recombination centers due to diffusion of In was suppressed, and the intensity of light emitted from QDs at room temperature increased about tenfold compared with the case without this control. Thus, requirement (iii) was satisfied.

4 Device operation

We verified the device operation at room temperature (300 K) by the μ-PL method. Since the photon energy needed to generate e–h pairs in the GaAs barrier layer is 1.44 eV, we used a cw semiconductor laser with a photon energy of 1.91 eV as a light source for P_{in1} of the AND gates and P_{es} of the NOT gates. The power of input light was 80 μW. Furthermore, we used an optical parametric oscillator (photon energy of 0.965 eV, pulse width of 100 fs, repetition frequency of 80 MHz, and input power of 40 μW) pumped by a Ti:sapphire laser and tuned to $E(\mathrm{QD1}{:}E_{0,\mathrm{h}}{-}E_{0,\mathrm{e}})$ of QD1 as a light source for P_{in2} of the AND gates and P_{in} of the NOT gates. The numerical aperture of the objective lens used for the μ-PL method was 0.6, and the spatial resolution was 500 nm.

Light (P_{in1}, P_{es}) from the cw semiconductor laser was made to enter the two-dimensional mesa array, and we measured the spatial distribution of the value of the ratio $R(=P_{\mathrm{out}}/P'_{\mathrm{out}})$ of the output signal power P_{out} in the case where the input signal (P_{in2}, P_{in}) was applied and the output signal power P'_{out} in the case where the input signal was not applied. According to [21], the contrast ratio C of a logic gate is defined as $C(\mathrm{dB}) = 10\log(P_{\mathrm{out,h}}/P_{\mathrm{out},l})$ using P_{out} in a high state ($P_{\mathrm{out,h}}$) and P_{out} in a low state ($P_{\mathrm{out},l}$). Thus, R described above is $R = 10^{C/10}$ for AND gates and $R = 10^{-C/10}$ for NOT gates. Figures 6(a) and (b) show the results of measurement of mesa structures having dimensions of 300 nm and 200 nm on each side, respectively. Here, P_{out} represents a value obtained by integrating the range of photon energy of 1.0533 to 1.0120 eV in the spectrum of the output signal. Spots of yellow to red represent the values of R for AND gates. On the other hand, darker spots of blue to black represent the values of R for NOT gates. Mesa structures having particularly distinct values of R are surrounded by white rings.

Since the values of R fluctuated by as much as 2.2% due to the background noise caused by deep level emission from the GaAs substrate, devices whose average value of C of mesa structures was greater than $10\log(1.025) = 0.11$ dB were defined as AND gates and NOT gates. At this time, in the case of the 300 nm × 300 nm mesa structures, of 133 mesa structures observed, 53 mesa structures operated as AND gates, 50 mesa structures operated as NOT gates, and there were 30 others. In the case of the 200 nm × 200 nm mesa structures, of 126 mesa structures observed, 36 mesa structures operated as AND gates, 36 mesa structures operated as NOT gates, and there were 54 others.

We verified experimentally that the enhancement factor of P_{out} by the 40 nm Au nanoparticle was 3. Furthermore, we excited all the mesa structures in the two-dimensional array with second harmonic generation (SHG) of the mode-locked Ti:sapphire laser and measured the relaxation lifetime of light emission with an avalanche photodiode. As a result, we confirmed that a fast relaxation component having a time constant of 50 ps appeared due to the 40 nm Au nanoparticle. This result suggests that the maximum operation frequency of the device with the Au nanoparticle disposed on the mesa structures is 1/50 ps (=20 GHz). This point will be published in detail on some other occasion.

5 Discussion

First, C of the device will be discussed. As will be understood from Figs. 6(a) and (b), the maximum value in the spatial distribution of C in the two-dimensional array was $10\log(1.15) = 0.61$ dB for AND gates and $10\log(0.85) = 0.71$ dB for NOT gates. However, these values are underestimated for two reasons: (i) The value obtained by integrating over the range of photon energy of 1.0533–1.0120 eV is used; (ii) Light in the form of short pulses having a low duty ratio and a low repetition frequency (100 fs, 80 MHz) is used as the input signals (P_{in2}, P_{in}).

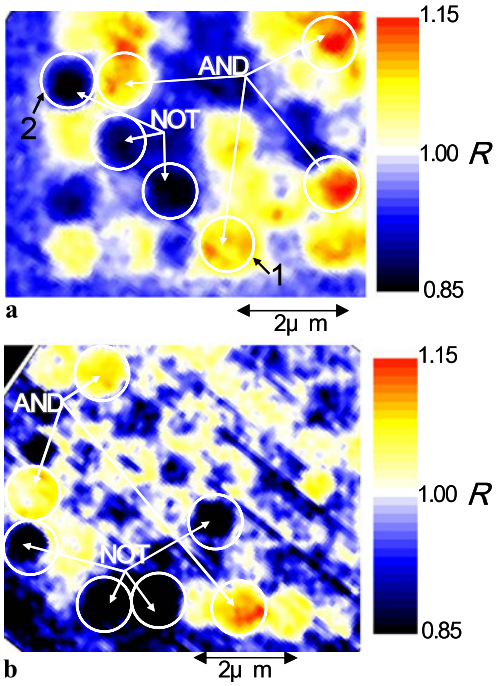

Fig. 6 Spatial distribution of the values of ratio R regarding the two-dimensional mesa array. (**a**) Mesa dimensions 300 nm × 300 nm and (**b**) mesa dimensions 200 nm × 200 nm

Now, reason (i) will be discussed in the context of the AND gate with ring number 1 and the NOT gate with ring number 2 in Fig. 6(a). Figure 7(a) shows the spectra of output light signals of the AND gate at the center of ring number 1 in a high state and a low state by a solid curve and a dashed curve, respectively. C becomes greatest at the position of the arrow in the figure, with a value of $10\ \log(2.0) = 3.0$ dB. Furthermore, Fig. 7(b) shows the spectra of output light signals of the NOT gate with ring number 2 in Fig. 6(a) in a high state and a low state by a solid curve and a dashed curve, respectively. C becomes greatest at the position of the arrow in the figure, again with a value of $10\log(2.0) = 3.0$ dB. Thus, by choosing the photon energy of P_{out} of each device so that C becomes greatest, C of AND gates and C of NOT gates increase by 2.4 $(=3.0 - 0.61)$ dB and 2.3 $(=3.0 - 0.71)$ dB, respectively.

Next, reason (ii) will be discussed. In the case where light having a high duty ratio is used as the input signals (P_{in2}, P_{in}), the values of C become greater. In the experiment described above, pulse signals are generated both in a high state and a low state. Since P_{out} occurs by recombination of electrons and holes in QD2, the time duration of the pulsed light signals is substantially equal to the recombination lifetime (measured value is 0.38 ns) of the electrons and holes in the device. Furthermore, the pulse repetition time is 12.5 ns (=1/80 MHz). That is, since the duty ratio is 0.38 ns/12.5 ns = 0.03, by using a light source with a pulse repetition time of 0.38 ns in the experiment and neglecting the effects of saturation, C of AND gates and NOT gates becomes 15 $(=10\log(1/0.03))$ dB greater compared with (i) above. From the discussion of reasons (i) and (ii), C of AND gates and NOT gates obtained as results of the experiment were both 18 $(=3 + 15)$ dB.

Next, the relationship between the transition energy between quantized energy levels of QDs constituting the device and the reproducibility of the device operation will be discussed. For this purpose, we fitted the spectrum of light emitted from QDs in each mesa structure with a Lorentzian curve and obtained the median of the transition energies of the individual QDs. Figures 8(a) to (c) show the results for AND gates, NOT gates, and other mesa structures, respectively. In Fig. 8(a), the red curve is a fitting curve for the spectrum of light emitted by recombination of electrons and holes through the $E_{0,\text{e}}$–$E_{0,\text{h}}$ transition in QD1. The blue curve is a fitting curve for the spectrum of light emitted by recombination of electrons and holes through the $E_{1,\text{e}}$–$E_{1,\text{h}}$ transition in QD1 and the $E_{0,\text{e}}$–$E_{0,\text{h}}$ transition in QD2 (corresponding to P_{out}). Furthermore, in Fig. 8(b), the red, green, and blue curves are fitting curves for the spectra of light emitted by recombination of electrons and holes through the $E_{0,\text{e}}$–$E_{0,\text{h}}$ transition in QD1, the $E_{1,\text{e}}$–$E_{1,\text{h}}$ transition in QD1, and the $E_{0,\text{e}}$–$E_{0,\text{h}}$ transition in QD2 (corresponding to P_{out}). The FWHM of the green curve is wider than that of the red curve. This is because the $E_{1,\text{e}}$–$E_{1,\text{h}}$ transition is fourfold degenerate, causing quick phase relaxation between degenerate levels, and because inter-sublevel relaxation of electrons and holes to the $E_{0,\text{e}}$ and the $E_{0,\text{h}}$ levels occurs quickly, whereby the FWHM of the spectrum of emitted light increases [14–16]. Figure 8(c) shows the spectrum of light emitted from the other mesa structures. We fitted the spectrum with multiple Lorentzian curves having different center positions.

Figure 9 shows the results of plotting the photon energies at the center positions of the Lorentzian curves obtained by the fitting described above as a function of R. The white triangles, white circles, and black squares in the figure correspond to AND gates ($R = 10^{C/10}$), NOT gates ($R = 10^{-C/10}$), and the other mesa structures, respectively. The white triangles and circles distributed in the vicinity of the red curve A represent the photon energies of light emission by recombination of electrons and holes through the $E_{1,\text{e}}$–$E_{1,\text{h}}$ transition in QD1. On the other hand, white triangles and circles distributed in the vicinity of the red curve B represent the photon energies of light emission by recombination of electrons and holes through the $E_{1,\text{e}}$–$E_{1,\text{h}}$ transition in QD1 and the $E_{0,\text{e}}$–$E_{0,\text{h}}$ transition in QD2.

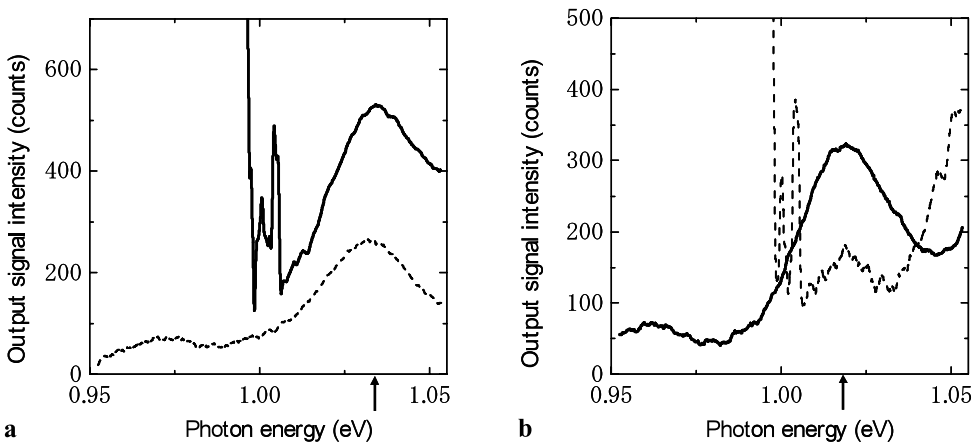

Fig. 7 Spectra of output signals. (**a**) Spectra of P_{out} of the AND gate with ring number 1 (*dashed curve* for low state ($P_{\text{out}} = 0$; $P_{\text{in1}} \neq 0$, $P_{\text{in2}} = 0$), *solid curve* for high state ($P_{\text{out}} \neq 0$; $P_{\text{in1}} \neq 0$, $P_{\text{in2}} \neq 0$)). (**b**) Spectra of P_{out} of the NOT gate with ring number 2 (*dashed curve* for low state ($P_{\text{out}} = 0$; $P_{\text{in}} \neq 0$), *solid curve* for high state ($P_{\text{out}} \neq 0$; $P_{\text{in}} = 0$))

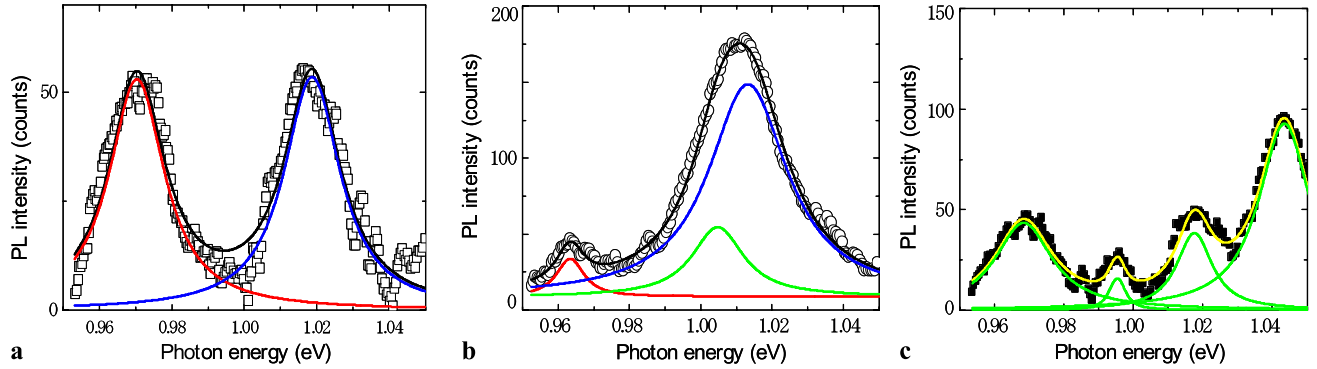

Fig. 8 Spectra of light emitted by different mesa structures. The *solid curves* represent the results of fitting with Lorentzian curves. (**a**) Mesa structures that operate as AND gates. (**b**) Mesa structures that operate as NOT gates. (**c**) Other mesa structures

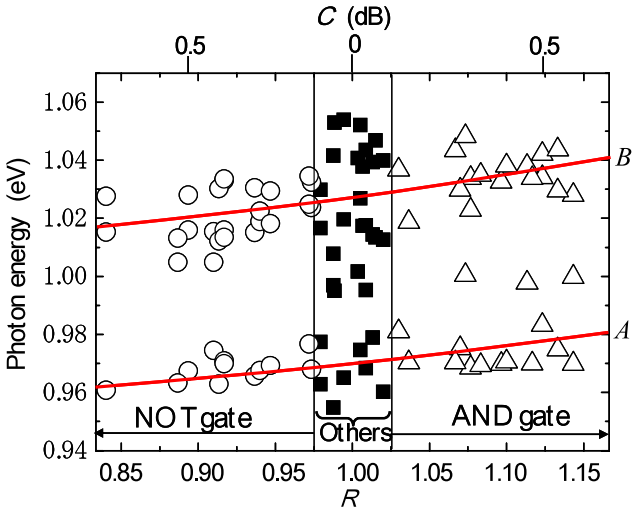

Fig. 9 Result of plotting the photon energies at the center positions of the Lorentzian curves obtained by the fitting shown in Fig. 8 as a function of R of individual mesa structures, together with the values of C. The *white triangles*, *white circles*, and *black squares* represent results obtained from the spectra of light emitted by AND gates, NOT gates, and the other mesa structures, respectively. The *curve A* represents the photon energy of $E(\mathrm{QD1}{:}E_{0,\mathrm{e}}{-}E_{0,\mathrm{h}})$, and the *curve B* represents the photon energy in which $E(\mathrm{QD1}{:}E_{1,\mathrm{e}}{-}E_{1,\mathrm{h}})$ and $E(\mathrm{QD2}{:}E_{0,\mathrm{e}}{-}E_{0,\mathrm{h}})$ overlap

As indicated by the black squares, mesa structures other than AND gates and NOT gates have a large number of peaks in the emitted light spectra, with the center positions of the Lorentzian curves considerably deviated from the red curves A and B. That is, the transition energies of two QDs in these mesa structures are not resonant or slightly off-resonant, and do not satisfy the operating conditions of AND gates or NOT gates. The differences in photon energy at the peaks were large, averaging at 42 meV. The probability of existence of a QD having a peak of light emission at such a photon energy position is greater than the probability of existence obtained from the value of the inhomogeneous width (31 meV) of the quantized energy level of QDs before the processing into mesa structures. That is, according to (1), the probability of existence of such a QD is estimated as 17% before the processing; whereas the measured value after the mesa processing was 30%. This is presumably attributable to changes in the quantized energy levels of QDs through the mesa processing. The changes presumably occur mainly in the periphery of mesa structures, where damage is likely to occur. Thus, by alleviating damage to QDs by adding a passivation regime in the mesa periphery, improvement in the device fabrication yield can be expected [22].

Finally, the meanings of "resonant" and "slightly off-resonant" device operation conditions described in Sect. 2 will be clarified, and it will be pointed out that the device operates by way of energy transfer via dressed photons instead of the ordinary Förster mechanism. Light emission by recombination of electrons and holes through the $E_{1,\mathrm{e}}{-}E_{1,\mathrm{h}}$ transition in QD1 and the $E_{0,\mathrm{e}}{-}E_{0,\mathrm{h}}$ transition in QD2 contribute to the white triangles and circles in the vicinity of the red curve B in Fig. 9. Thus, two Lorentzian curves overlap. Figure 10 shows the results of plotting the energy difference $E(\mathrm{QD2}{:}E_{0,\mathrm{e}}{-}E_{0,\mathrm{h}}) - E(\mathrm{QD1}{:}E_{1,\mathrm{e}}{-}E_{1,\mathrm{h}})$ between the peaks of the two Lorentzian curves for AND gates and NOT gates. White circles in the figure are distributed in a range of the absolute value of $E(\mathrm{QD2}{:}E_{0,\mathrm{e}}{-}E_{0,\mathrm{h}}) - E(\mathrm{QD1}{:}E_{1,\mathrm{e}}{-}E_{1,\mathrm{h}})$ between 10 and 20 meV. Thus, it is understood that "slightly off-resonant," which is to be satisfied by $E(\mathrm{QD1}{:}E_{1,\mathrm{e}}{-}E_{1,\mathrm{h}})$ and $E(\mathrm{QD2}{:}E_{0,\mathrm{e}}{-}E_{0,\mathrm{h}})$ of two QDs constituting a NOT gate, refers to a state of detuning from resonance by approximately 10 to 20 meV. On the other hand, as for AND gates, as indicated by white triangles in the figure, of 14 devices examined, $E(\mathrm{QD2}{:}E_{0,\mathrm{e}}{-}E_{0,\mathrm{h}}) - E(\mathrm{QD1}{:}E_{1,\mathrm{e}}{-}E_{1,\mathrm{h}}) = 0$ (i.e., separation by fitting was not possible due to their homogeneous broadening) for 11 devices. By comparing these values, it is understood that $E(\mathrm{QD1}{:}E_{1,\mathrm{e}}{-}E_{1,\mathrm{h}})$ and $E(\mathrm{QD2}{:}E_{0,\mathrm{e}}{-}E_{0,\mathrm{h}})$ are resonant with each other and QD1 and QD2 operate as an AND gate if $E(\mathrm{QD1}{:}E_{1,\mathrm{e}}{-}E_{1,\mathrm{h}})$ and $E(\mathrm{QD2}{:}E_{0,\mathrm{e}}{-}E_{0,\mathrm{h}})$ are close

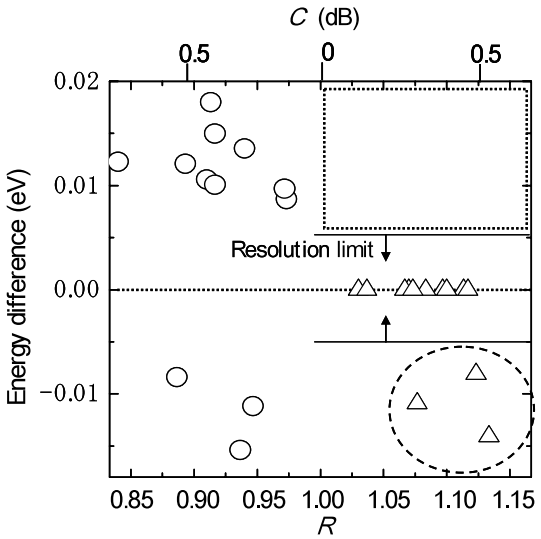

Fig. 10 Result of plotting the energy difference $E(\mathrm{QD2}{:}E_{0,\mathrm{e}}{-}E_{0,\mathrm{h}}) - E(\mathrm{QD1}{:}E_{1,\mathrm{e}}{-}E_{1,\mathrm{h}})$ of peaks of light emission along the *curve B* in Fig. 9 as a function of R of individual mesa structures, together with the values of C. The *white triangles* represent AND gates, and the *white circles* represent NOT gates

enough to each other that these energies are inseparable due to their homogeneous broadenings.

The devices indicated by three white triangles in a broken ellipse in Fig. 10 are considered to operate as AND gates by resonance between the energy $E(\mathrm{QD1}{:}E_{1,\mathrm{e}}{-}E_{0,\mathrm{h}})$ of the electric dipole-forbidden transition ($E_{1,\mathrm{e}}{-}E_{0,\mathrm{h}}$ transition) in QD1 and the energy $E(\mathrm{QD2}{:}E_{0,\mathrm{e}}{-}E_{0,\mathrm{h}})$ of the electric dipole-allowed transition ($E_{0,\mathrm{e}}{-}E_{0,\mathrm{h}}$ transition) in QD2 instead of the operation condition $E(\mathrm{QD2}{:}E_{0,\mathrm{e}}{-}E_{0,\mathrm{h}}) - E(\mathrm{QD1}{:}E_{1,\mathrm{e}}{-}E_{1,\mathrm{h}}) = 0$. This is because of the following two reasons: (i) The photon energy of $E(\mathrm{QD1}{:}E_{1,\mathrm{e}}{-}E_{0,\mathrm{h}})$ of the electric dipole-forbidden transition estimated on the basis of the band offset of InAs and GaAs [23] is 11 meV lower than that of $E(\mathrm{QD1}{:}E_{1,\mathrm{h}}{-}E_{1,\mathrm{e}})$. This value substantially coincides with the value of $E(\mathrm{QD2}{:}E_{0,\mathrm{e}}{-}E_{0,\mathrm{h}}) - E(\mathrm{QD1}{:}E_{1,\mathrm{e}}{-}E_{1,\mathrm{h}})$ of the devices indicated by the three white triangles in the broken ellipse in Fig. 10. (ii) We were unable to find AND gates in the region where electric dipole-forbidden transitions as in (i) above are absent ($E(\mathrm{QD2}{:}E_{0,\mathrm{e}}{-}E_{0,\mathrm{h}}) - E(\mathrm{QD1}{:}E_{1,\mathrm{e}}{-}E_{1,\mathrm{h}}) > 0$; the dotted rectangular region at the upper right part of Fig. 10). The occurrence of energy transfer via electric dipole-forbidden transitions indicates that the device operates through energy transfer between QDs via exchange of dressed photons instead of the ordinary Förster mechanism [1, 11].

6 Conclusions

By using mesa structures of InAs QDs, we succeeded for the first time in fabricating nanophotonic logic gates that operated at room temperature. The mesa dimensions were 300 nm × 300 nm × 85 nm and 200 nm × 200 nm × 85 nm, and the mesa structures were arrayed two-dimensionally on a GaAs substrate at an areal density of 1×10^8 cm^{-2}. A device is formed of two quantum dots vertically aligned in a mesa structure. Of 133 mesa structures having dimensions of 300 nm on each side, 53 operated as AND gates and 50 operated as NOT gates. Of 126 devices having dimensions of 200 nm on each side, 36 operated as AND gates and 36 operated as NOT gates. In order to fabricate a NOT gate, the absolute value of the energy difference between $E(\mathrm{QD2}{:}E_{0,\mathrm{e}}{-}E_{0,\mathrm{h}})$ and $E(\mathrm{QD1}{:}E_{1,\mathrm{e}}{-}E_{1,\mathrm{h}})$ must be 10 to 20 meV. On the other hand, an AND gate operates if $E(\mathrm{QD2}{:}E_{0,\mathrm{e}}{-}E_{0,\mathrm{h}}) = E(\mathrm{QD1}{:}E_{1,\mathrm{e}}{-}E_{1,\mathrm{h}})$, and also operates if the condition $E(\mathrm{QD2}{:}E_{0,\mathrm{e}}{-}E_{0,\mathrm{h}}) = E(\mathrm{QD1}{:}E_{1,\mathrm{e}}{-}E_{0,\mathrm{h}})$ is satisfied, even in the condition of an electric dipole-forbidden transition. By precisely controlling the quantized energy levels of QDs through optimization of the mesa processing and use of the photo-assisted size-controlled growth [24], the device fabrication yield is expected to improve even further.

Acknowledgement This paper belongs to "Innovative nanophotonics components development project" which OITDA contracted with The New Energy and Industrial Technology Development Organization (NEDO) since 2006.

References

1. M. Ohtsu, T. Kawazoe, T. Yatsui, M. Naruse, IEEE J. Sel. Top. Quantum Electron. **14**, 1404 (2008)
2. T. Kawazoe, K. Kobayashi, S. Sangu, M. Ohtsu, Appl. Phys. Lett. **82**, 2957 (2003)
3. T. Yatsui, S. Sangu, T. Kawazoe, M. Ohtsu, S.J. An, J. Yoo, G.C. Yi, Appl. Phys. Lett. **90**, 223110 (2007)
4. T. Kawazoe, K. Kobayashi, K. Akahane, M. Naruse, N. Yamamoto, M. Ohtsu, Appl. Phys. B: Laser Opt **84**, 243 (2006)
5. S. Sangu, K. Kobayashi, A. Shojiguchi, M. Ohtsu, Phys. Rev. B **69**, 115334 (2004)
6. M. Naruse, H. Hori, K. Kobayashi, P. Holmstrom, L. Thylen, M. Ohtsu, Opt. Express **18**, A544 (2010)
7. T. Kawazoe, K. Kobayashi, S. Takubo, M. Ohtsu, J. Chem. Phys. **122**, 024715 (2005)
8. H. Yonemitsu, T. Kawazoe, K. Kobayashi, M. Ohtsu, J. Lumin. **122–123**, 230 (2007)
9. T. Yatsui, K. Hirata, W. Nomura, Y. Tabata, M. Ohtsu, Appl. Phys. B **93**, 55 (2008)
10. K. Kobayashi, A. Sato, T. Yatsui, T. Kawazoe, M. Ohtsu, Appl. Phys. Express **2**, 075504 (2009)
11. T. Kawazoe, K. Kobayashi, J. Lim, Y. Narita, M. Ohtsu, Phys. Rev. Lett. **88**, 067404 (2002)
12. K. Kobayashi, S. Sangu, T. Kawazoe, M. Ohtsu, J. Lumin. **112**, 117 (2005)
13. T. Kawazoe, K. Kobayashi, M. Ohtsu, Appl. Phys. Lett. **86**, 103102 (2005)
14. G.A. Narvaez, A. Zunger, Phys. Rev. B **74**, 045316 (2006)
15. K.H. Schmidt, G. Medeiros-Ribeiro, M. Oestreich, P.M. Petroff, Phys. Rev. B **54**, 11346 (1996)
16. L. He, G. Bester, Z. Su, A. Zunger, Phys. Rev. B **76**, 035313 (2007)

17. S. Guha, A. Madhukar, K.C. Rajkumar, Appl. Phys. Lett. **57**, 2110 (1990)
18. V. Zwiller, H. Blom, P. Jonsson, N. Panev, S. Jeppesen, T. Tsegaye, E. Goobar, M.E. Pistol, L. Samuelson, G. Björk, Appl. Phys. **78**, 2476 (2001)
19. Z. Mi, P. Bhattacharya, J. Appl. Phys. **98**, 023510 (2005)
20. P. Borri, W. Langbein, J. Mørk, J.M. Hvam, F. Heinrichsdorff, M.-H. Mao, D. Bimberg, Phys. Rev. B **60**, 7784 (1999)
21. F. Yu, J. Suganda, Y. Shizuhuo (eds.), *Introduction to Information Optics* (Academic Press, San Diego/London, 2001), p. 202
22. R. Dylewicza, R.M. De La Rue, R. Wasielewski, P. Mazur, G. Mezősi, A.C. Bryce, J. Vac. Sci. Technol. B **28**, 882 (2010)
23. D.J. Arent, K. Deneffe, C. Van Hoof, J. De Boeck, G. Borghs, J. Appl. Phys. **66**, 1739 (1989)
24. T. Yatsui, M. Ohtsu, Appl. Phys. Lett. **95**, 043104 (2009)